New Nonlinear Ultrasonic Method for Material Characterization: Codirectional Shear Horizontal Guided Wave Mixing in Plate

Shengbo Shan[1,2], Mostafa Hasanian[1], Hwanjeong Cho[1], Cliff J. Lissenden[1,*] and Li Cheng[2]

[1] Department of Engineering Science and Mechanics, Penn State, State College, PA, USA, 16802

[2] Department of Mechanical Engineering, The Hong Kong Polytechnic University, Kowloon, Hong Kong.

* Corresponding author: lissenden@psu.edu

Abstract

A nonlinear ultrasonic method is proposed based on a group of newly discovered wave triplets where two primary codirectional shear-horizontal SH0 waves mix in a weakly nonlinear plate and generate a cumulative S0 Lamb wave at the sum frequency. Theoretical analyses show that any combination of two primary SH0 waves whose frequencies sum to the frequency at which the SH0 mode intersects the S0 Lamb wave mode results in an internally resonant secondary S0 Lamb wave. Moreover, the relationship between the frequency combination and the nonlinear Lamb wave generation efficiency is revealed, which guides further engineering applications. Finite element validations are carried out with the aid of a subtraction method for the nonlinear feature extraction. The cumulative effect of the generated S0 Lamb wave at the sum frequency as well as the influence of the frequency combinations on the nonlinear Lamb wave generation efficiency is confirmed. Experiments are performed to validate the proposed method as well as demonstrate its use for material characterization. The experiments require a gel filter to mitigate the influence of the undesired nonlinear sources. With the gel filter, the cumulative effect of the secondary S0 Lamb wave is verified and the corresponding slope is extracted and further used to characterize the material status of the fatigue samples. Results demonstrate the proposed method provides high sensitivity to early fatigue damage, which makes it promising for the further early damage detection applications.

Keywords: Shear-horizontal waves, Lamb waves, codirectional wave mixing, material characterization

1. Introduction

When a monochromatic ultrasonic wave propagates in a weakly nonlinear solid material, nonlinear

components at other frequencies occur [1-3]. Inherent with the material nonlinearity, these nonlinear ultrasonic waves show exceptional sensitivity to the material microstructure, thus enabling the detection of structural damage at an early stage, which is extremely powerful for nondestructive evaluation (NDE) [4-7].

In the NDE field, two techniques associated with nonlinear ultrasonic waves are widely investigated; second harmonic generation (self-interaction) [e.g., 3, 4, 8-10] and nonlinear wave mixing (mutual interaction) [e.g., 2, 11, 12]. The former is based on nonlinear wave generation at double the frequency of the propagating primary waves, while the latter uses the nonlinear waves at the sum or difference frequency of the two interacting primary waves. Compared to the second harmonic generation technique, the one based on nonlinear wave mixing has two appealing advantages for NDE applications. First, it is immune to the instrumentation nonlinearities if the two primary waves are independently excited in the system [13, 14]. Second, it provides more flexibility in designing the wave interactions for either global or local damage detection in structures, which is determined by the different wave mixing patterns like codirectional, counter-propagating and non-collinear [15-18].

Studies on the nonlinear wave mixing method can be traced back to more than 50 years ago when Jones and Kobett derived a criterion for the occurrence of strong nonlinear waves at sum and difference frequencies resulting from mixing two bulk waves in nonlinear solids [11]. More recently, wave mixing was used to detect low-cycle fatigue damage and quasi-static plastic deformation, demonstrating its feasibility in the NDE applications [2]. The technique was further extended to the mixing of Rayleigh waves, e.g., Kalyanasundaram proposed the nonlinear theory of the mixing of two codirectional Rayleigh waves [19]. Morlock *et al.* proposed a theoretical model to investigate the mixing of two Rayleigh surface waves for cumulative nonlinear wave generation, which was further validated by finite element (FE) simulations and experiments [13].

To be more relevant to engineering structures, the technique was extended to ultrasonic guided wave cases in isotropic plates and cylinders [20-24]. Recently, Hasanian and Lissenden [24] developed a general theoretical method for both collinear and noncollinear guided wave mixing in plates. Vector and dispersion analyses were combined to identify two interacting wave modes, frequencies, and directions

that generate secondary propagating waves at the sum or difference frequency. Finite element simulations of counter-propagating wave mixing and the associated experiments demonstrated the capability of wave mixing for localized material degradation [17]. Then the internal resonance criteria were formulated for the general problem of wave mixing at arbitrary angles in a plate and a simplified analytical model was proposed to account for wave mixing zones of finite size. The analytical model is applied to assess the influence of group velocity mismatch on the nonlinear wave amplitude [24].

The present study investigates mixing codirectional SH0 waves, whose interaction generates S0 Lamb waves at the sum frequency. As in the case of counter-propagating SH0 wave mixing [17], any frequencies that sum to the value prescribed by the dispersion analysis are usable. The difference is that while counter-propagating waves provide advantages for the detection of localized material degradation by scanning, the wave mixing zone is necessarily small, potentially limiting generated nonlinear wave energy. Codirectional mixing of SH0 waves has the advantage of a large wave mixing zone, resulting in more power flux to the secondary S0 waves that should be better measured where material degradations globally occur. In addition, the cumulative effect which only attributes to material nonlinearity can be more easily used as an indicator of material degradation. Such cumulative-effect-based method should be less vulnerable to other undesired nonlinear sources. An NDE method is proposed to characterize material degradation.

To reveal the characteristics of the proposed method, the remainder of the paper is organized as follows. Theories for guided wave mixing in weakly nonlinear plates are briefly summarized and then the influence of different frequency combinations on the secondary S0 wave generation efficiency is evaluated in Sec. 2. A finite element model is established in Sec. 3, along with a subtraction method to isolate the nonlinearity associated with mutual wave interaction. The highlighted wave triplets are validated in terms of their cumulative secondary wave generation, as well as the influence of the frequency combinations on the nonlinear wave amplitude. Sec. 4 describes the laboratory experiments and the application of the proposed method. Specifically, a gel filter is proposed to mitigate the undesired nonlinear Lamb wave responses in the system. With the aid of the gel filter, the source of the measured nonlinearity is limited to the waveguide material. The sensitivity of the method is demonstrated for

fatigue damage, where a significant change in nonlinearity occurs between 0-25% of the fatigue life. Finally, Sec. 5 concludes the paper and addresses the appealing characteristics of the proposed method.

2. Theories

Determination of meaningful experimental test parameters would not be possible without understanding the nuances of nonlinear guided wave propagation. In this section, theories on the nonlinear guided waves generated by the mixing of two colinear primary waves in a weakly nonlinear plate are briefly summarized with emphasis on the internal resonance criteria for cumulative secondary wave generation. Based on these criteria, selection of the corresponding wave triplets is discussed, highlighting a group where the mixing of two codirectional SH0 waves generates S0 Lamb waves at the sum frequency. In addition, the influence of the frequency combinations of the primary SH0 waves on the efficiency of secondary wave generation is further discussed and evaluated.

2.1 Wave triplets for the cumulative nonlinear generation

To proceed, the stress-strain relation of an isotropic nonlinear elastic material characterized by the Landau-Lifshitz model is introduced,

$$\mathbf{T^{RR}} = \lambda tr[\mathbf{E}]\mathbf{I} + 2\mu\mathbf{E} + \overline{A}\mathbf{E}^2 + \overline{B}tr[\mathbf{E}^2]\mathbf{I} + 2\overline{B}tr[\mathbf{E}]\mathbf{E} + \overline{C}(tr[\mathbf{E}])^2\mathbf{I} \tag{1}$$

where λ and μ are Lamé constants and $\overline{A}$, $\overline{B}$, $\overline{C}$ are the Landau third-order elastic constants (TOECs). $\mathbf{I}$ is the second rank identity tensor and the operation $tr[\ ]$ represents the trace. $\mathbf{T^{RR}}$ denotes the second Piola-Kirchhoff stress tensor. $\mathbf{E}$ is the Lagrangian strain tensor, which is defined in terms of the displacement gradient, $\mathbf{H} = \nabla\mathbf{u}$, as

$$\mathbf{E} = \frac{1}{2}(\mathbf{H} + \mathbf{H}^T + \mathbf{H}^T\mathbf{H}). \tag{2}$$

In a weakly nonlinear elastic plate, the nonlinear wave components are much smaller than the primary waves. Therefore, the perturbation theory can be applied to decouple the system into linear and nonlinear

parts. The governing equations for wave generation problems are more naturally written with the first Piola-Kirchhoff stress tensor **S** which relates to the second Piola-Kirchhoff stress tensor through the deformation gradient (**I**+**H**). Correspondingly, the stresses can be decomposed as,

$$\mathbf{S} = \mathbf{S}^L + \mathbf{S}^{NL} = (\mathbf{I} + \mathbf{H})\mathbf{T}^{RR} \tag{3}$$

$$\mathbf{S}^L = \lambda tr[\mathbf{H}]\mathbf{I} + \mu(\mathbf{H} + \mathbf{H}^T) \tag{4}$$

$$\mathbf{S}^{NL} = \left(\frac{\lambda}{2}tr[\mathbf{H}^T\mathbf{H}] + \overline{C}(tr[\mathbf{H}])^2\right)\mathbf{I} + \overline{B}tr[\mathbf{H}]\mathbf{H}^T + \frac{\overline{A}}{4}\mathbf{H}^T\mathbf{H}^T + \frac{\overline{B}}{2}tr[\mathbf{HH} + \mathbf{H}^T\mathbf{H}]\mathbf{I}$$
$$+ (\lambda + \overline{B})tr[\mathbf{H}]\mathbf{H} + \left(\mu + \frac{\overline{A}}{4}\right)(\mathbf{HH} + \mathbf{H}^T\mathbf{H} + \mathbf{HH}^T) \tag{5}$$

where the superscripts L and NL represent the linear and nonlinear parts respectively. It is worth noting that the nonlinear stresses can be calculated by substituting the linear displacement gradients into Eq. (5); it is these nonlinear stresses that are responsible for the generation of nonlinear waves.

Consider two collinear primary waves a and b propagating in the X direction in a $2h$ thick plate. Relevant coordinates and wave polarizations are sketched in Fig. 1(a). The wave fields can be expressed in terms of the displacements as

$$\mathbf{u}_a(X, Y, Z) = A_a\mathbf{U}_a(Z)e^{i(k_aX-\omega_at)} \tag{6}$$

$$\mathbf{u}_b(X, Y, Z) = A_b\mathbf{U}_b(Z)e^{i(k_bX-\omega_bt)} \tag{7}$$

where $\mathbf{U}(Z)$ is the normalized displacement distribution in the Z direction; i.e., the wave structure. Respectively, k and ω are the wave number and the angular frequency of the primary waves. k is related to ω by the phase velocity as $k = \omega/c_{phase}$. The wave number can be either positive or negative, representing different wave propagating directions. A denotes the amplitude of the displacement field. After substituting the displacement gradients of the mixed wave field $(\mathbf{u}_a + \mathbf{u}_b)$ into Eq. (5), the nonlinear stresses can be obtained where some terms contain functions of $e^{i((k_a\pm k_b)X-(\omega_a\pm\omega_b)t)}$ and $e^{-i((k_a\pm k_b)X-(\omega_a\pm\omega_b)t)}$. These terms indicate that new wave components at the sum and difference

frequencies are generated through the mixing of the two primary waves. According to the normal mode expansion method, these generated nonlinear wave components can be expressed as

$$\mathbf{u}_{ab} = \frac{1}{2}\sum_{m=1}^{N} A_m(X)\, \mathbf{U}_m(Z) e^{-i((\omega_a \pm \omega_b)t)} \tag{8}$$

where $A_m(X)$ is the modal amplitude of the mth wave mode. Upon applying the reciprocity theorem [25], the modal amplitude can be obtained as [20, 24]

$$A_m(X) = \begin{cases} -\dfrac{i\left(f_m^{surf}+f_m^{vol}\right)}{4P_{mm}\left(k_m^*-(k_a\pm k_b)\right)}\left(e^{ik_m^* X} - e^{i(k_a \pm k_b)X}\right) & \text{if } k_m^* \neq k_a \pm k_b \\ \dfrac{\left(f_m^{surf}+f_m^{vol}\right)}{4P_{mm}} X e^{i(k_a \pm k_b)X} & \text{if } k_m^* = k_a \pm k_b \end{cases} \tag{9}$$

where k_m^* is the complex conjugate of the wave number k_m corresponding to the nonlinear wave expected to be generated. The terms f_m^{surf} and f_m^{vol} are the nonlinear driving forces that transfer power from the primary waves to the secondary waves through the surface and volume respectively. In addition, P_{mm} is related to the Poynting vector component in the wave propagation direction by the modal velocity $\mathbf{V}_m$ and stress $\mathbf{S}_m$.

$$f_m^{surf} = -\frac{1}{2}\mathbf{S}^{NL}(\boldsymbol{a},\boldsymbol{b})\mathbf{V}_m^*(Z) \cdot \mathbf{n}_Z|_{-h}^h \tag{10}$$

$$f_m^{vol} = \frac{1}{2}\int_{-h}^{h} Div[\mathbf{S}^{NL}(\boldsymbol{a},\boldsymbol{b})] \cdot \mathbf{V}_m^*(Z)\, \mathrm{d}Z \tag{11}$$

$$P_{mm} = -\frac{1}{4}\int_{-h}^{h}\left(\frac{\mathbf{S}_m(Z)\mathbf{V}_m^*(Z)+\mathbf{V}_m(Z)\mathbf{S}_m^*(Z)}{2}\right) \cdot \mathbf{n}_X\, \mathrm{d}Z \tag{12}$$

where $S^{NL}(a, b)$ corresponds to the nonlinear stresses associated with the mutual wave interaction and are given in the Appendix. Similar terms exist for self-interaction, but are not included here for clarity. Detailed equation derivations can be found in [17, 21, 24]. Equation (9) indicates that internal resonance will occur and the amplitude of the nonlinear waves will be linearly cumulative with respect to the propagation distance if two criteria are satisfied, i.e.:

(i) nonzero power flux, $f_m^{surf} + f_m^{vol} \neq 0$; (13)

(ii) phase matching, $k_m = k_a \pm k_b$. (14)

Guided by these internal resonance criteria, Eqs. (13) and (14), the wave triplets for cumulative nonlinear generation can be identified. Some representative ones are identified in [17, 24] associated with specific frequencies and mode types. Counter-propagating SH0 were investigated to detect localized material nonlinearity by scanning, but here we aim to increase the wave interaction zone by using codirectional waves.

Guided by the internal resonance criteria, one specific group of wave triplets is investigated; i.e., the mixing of two codirectional primary SH0 waves to generate a secondary S0 mode Lamb wave at the sum frequency, as sketched in Fig. 1(a). This group of wave triplets is exemplified by a typical case shown in Fig. 1(b), with two primary SH0 wave modes at 2.34 MHz-mm and 1 MHz-mm respectively to generate the S0 Lamb wave at 3.34 MHz-mm in an aluminum plate given the properties in Table 1. This group of wave triplets only requires that the sum frequency occurs at the intersection of the SH0 and S0 phase velocity dispersion curves, giving various options for the frequency combinations of the primary waves. The variability offers great flexibility for the measurement system design within the specific NDE application.
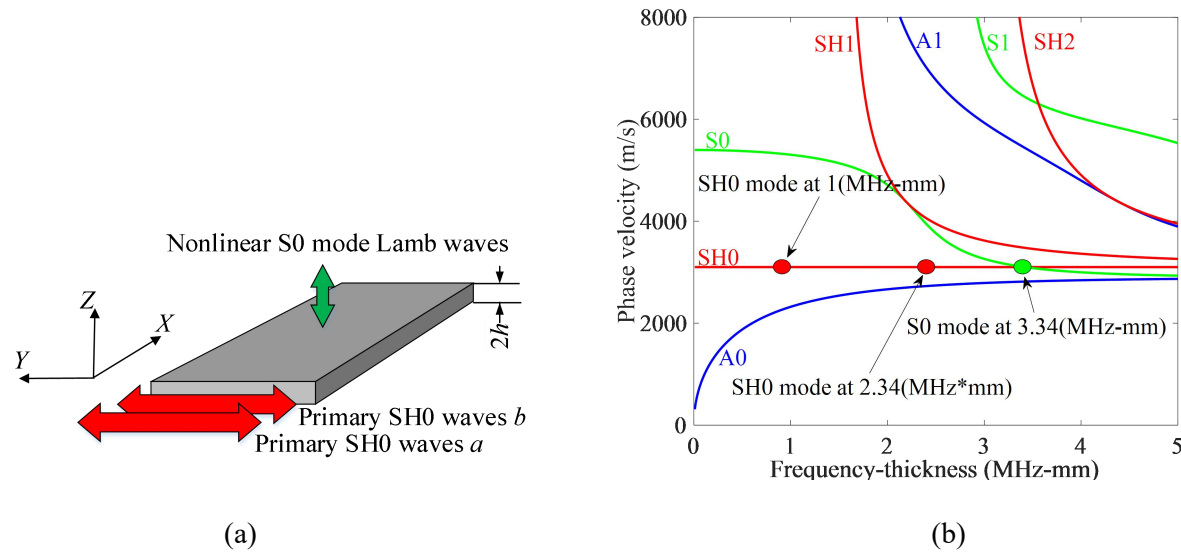
Fig. 1. (a) sketch of codirectional SH wave mixing and the coordinates; (b) an example of the highlighted wave triplets plotted on the dispersion curves of an aluminum plate.

2.2 Influence of the frequency combinations

As just observed, codirectional mixing of SH0 waves to generate the S0 mode at the sum frequency as shown in Fig. 1(b) is constrained only by the sum frequency being at the SH0-S0 mode intersection point, i.e.,

$$2f_a h + 2f_b h = 3.34 \text{ MHz-mm}. \tag{15}$$

Since there are many options for the combination of the primary frequencies in this specific group of wave triplets, it is beneficial to assess which combination is the most efficient. Two aspects of this group of wave triplets make an analytical study fruitful:

(i) the SH0 wavestructure is uniform through the thickness and only involves one component;

(ii) all combinations of primary waves will generate the secondary S0 mode at the same frequency-thickness product, thus there is only one secondary wavestructure of concern.

The modal amplitude of the secondary waves only depends on the nonlinear driving forces defined in Eqs. (10) and (11). As shown in the Appendix, the amplitude of the secondary S0 wave generated by two codirectionally-mixing planar SH0 waves can be written as

$$A_{ab} = C(A_a A_b)(k_a k_b)X \tag{16}$$

where A_a and A_b are the displacement amplitudes of primary SH0 waves and C is a parameter that depends only on the material parameters ($\lambda, \mu, \bar{A},$ and $\bar{B}$), velocity wavestructure, and Poynting vector as given in Eq. (A13). To characterize the nonlinear wave generation efficiency, consider a relative nonlinear parameter β' that is widely used in the literature [2, 26-30]

$$\beta' = \frac{A_{ab}}{A_a A_b}. \tag{17}$$

In practice, the amplitudes of different wave fields can be used in this equation; e.g., displacements, stresses, and sensed voltages. Herein, the displacement amplitudes are used to characterize the nonlinear wave generation efficiency. Therefore, the β' for different frequency combinations can be further simplified by substituting Eq. (16) into Eq. (17),

$$\beta' = C k_a k_b X. \tag{18}$$

As noted above, since the SH0 waves are nondispersive, $k_a + k_b$ is constant for any combination of primary waves based on Eq. (15). Therefore, β' is larger when the two frequencies get closer together. This finding may potentially provide guidance for further system design in NDE applications.

3. Finite element studies

A finite element model is created to confirm the highlighted wave triplets for the generation of secondary waves at the sum frequency with the aid of a subtraction method. In addition, the influence of the primary frequency combinations on the nonlinear wave generation efficiency is evaluated.

3.1 The finite element model

The finite element model is established in Abaqus/Explicit as shown in Fig. 2. Laboratory experiments are reported for an aluminum plate, 200 mm long and 3.125 mm thick, in Section 4 and the same plate is

studied here. Periodic boundary conditions are applied in the Y direction along the lateral surfaces so that plane waves can be generated, simplifying the analysis [31]. Dynamic displacements are prescribed in the Y direction at one end of the plate to excite the primary SH waves. Displacements are uniformly applied through the thickness (Z direction) of the plate to match the wave structure of the SH0 waves. The mesh size is set to 0.1 mm, which ensures more than 30 elements per smallest wavelength. A time step of 10 ns is used to guarantee more than 80 points for the shortest time period. The Landau-Lifshitz hyperelastic material model is implemented through a VUMAT user subroutine. The material parameters for aluminum are listed in Table 1: mass density, Lamé constants and Landau third-order elastic constants. Due to the different polarization characteristics of the primary SH waves and the secondary Lamb waves, the displacements in the Y direction are recorded to characterize the SH waves, while the Z-direction displacements are recorded to represent the Lamb waves. The S0 Lamb waves at $fd = 3.34$ MHz-mm have both U_X and U_Z displacement components. U_Z is maximum on the surface and is approximately 83% of the maximum U_X, which occurs at the midplane. In addition, it is U_Z on the surface that is sensed in the experiments.
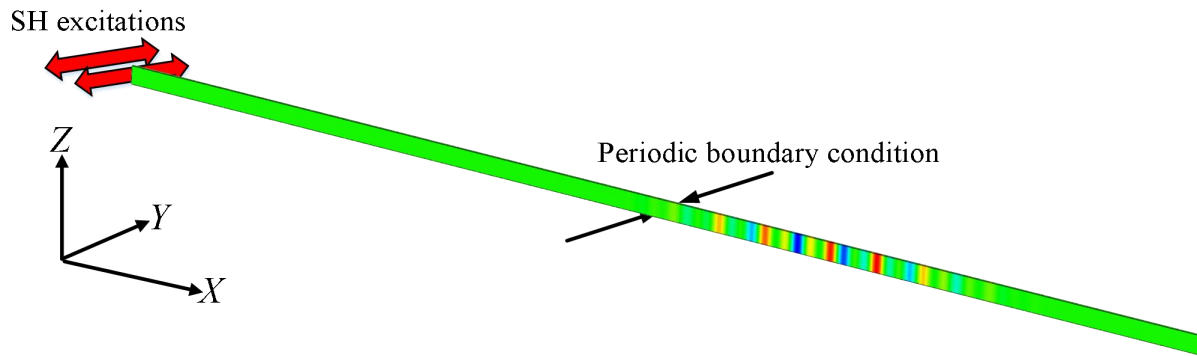

Fig. 2. The finite element model.

Table 1. Parameters of the aluminum used in the FE model

| ρ(kg/m³)	λ (GPa)	μ (GPa)	$\overline{A}$ (GPa)	$\overline{B}$ (GPa)	$\overline{C}$ (GPa)
2700	55.27	25.95	-351.2	-149.4	-102.8

3.2 A subtraction method

SH waves can generate symmetric Lamb waves at double the excitation frequency [10]. To isolate the S0 Lamb waves generated from mutual interactions of the SH waves from the symmetric Lamb waves generated from self interaction of the SH waves, a subtraction method [17] using three independent tests is adopted. First, both primary SH0 waves a and b having frequencies f_a and f_b are sent into the plate and the corresponding signal is designated as S_{A+B}. Then, primary waves a alone are excited, followed by primary waves b alone, giving the resultant signals S_A and S_B respectively. Finally, the difference signal is calculated:

$$S_{diff} = S_{A+B} - (S_A + S_B) \tag{19}$$

The difference signal S_{diff} contains only the nonlinearity associated with the mutual interaction of waves a and b. In the simulations, $f_a = 0.75$ MHz and $f_b = 0.32$ MHz are used, which correspond to the frequencies shown in Fig. 1(b). The amplitudes of the two primary waves are 10 nm. The signals at a point 60 mm away from the excitation are recorded in each of the three tests, then U_Y and U_Z are plotted in Fig. 3. The difference signal S_{diff} is also plotted for each displacement component. The in-plane displacements U_Y corresponding to the SH waves in Fig. 3(a) indicate the two primary waves thoroughly mix during propagation as they have the same phase and group velocities. Fig. 3(b) shows the out-of-plane displacements U_Z associated with the generated Lamb waves. Note that the amplitude units are pm in Fig. 3(b) and nm in Fig. 3(a). Clearly, the signals associated with self interaction for S_A and S_B are significantly smaller than those for mutual interaction for S_{A+B} and S_{diff}. It is also observed that the Lamb wave signals in Fig. 3(b) arrive later than the SH wave signals in Fig. 3(a), indicating that the Lamb waves have a slower group velocity than the SH waves, which is well-known (2395 m/s for S0 Lamb waves at this frequency and 3100 m/s for SH0 waves). By taking the Fast Fourier Transform (FFT) of the windowed wave packages in Fig. 3(b), the frequency spectra of the wave packages are obtained and shown in Fig. 3(c) and (d). The plots demonstrate the difference between the internally resonant secondary waves ($f_a + f_b$) and those that are not phase matched ($2f_a$, $2f_b$, f_a - f_b) is an order of magnitude or more at this position. In addition, it shows that the subtraction method eliminates the frequency content
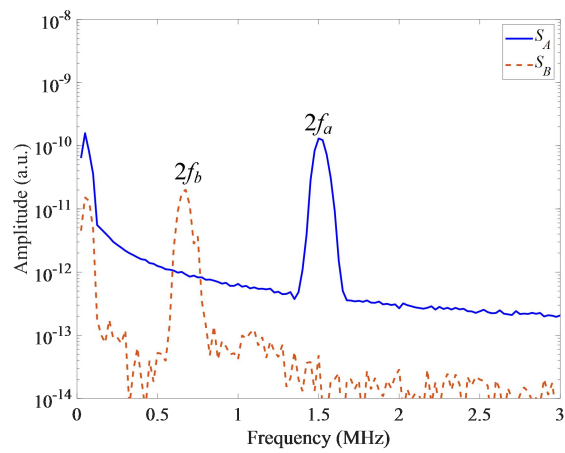
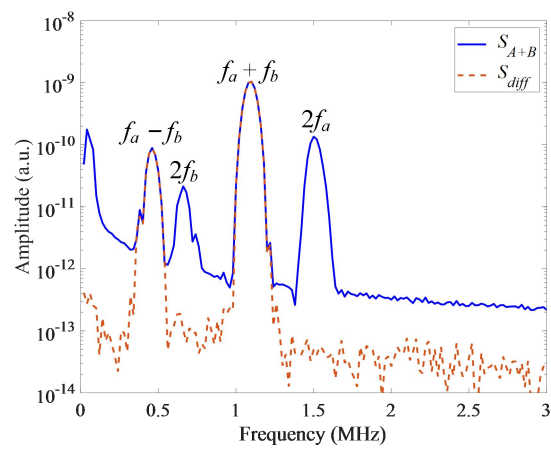associated with self-interaction.

(a)
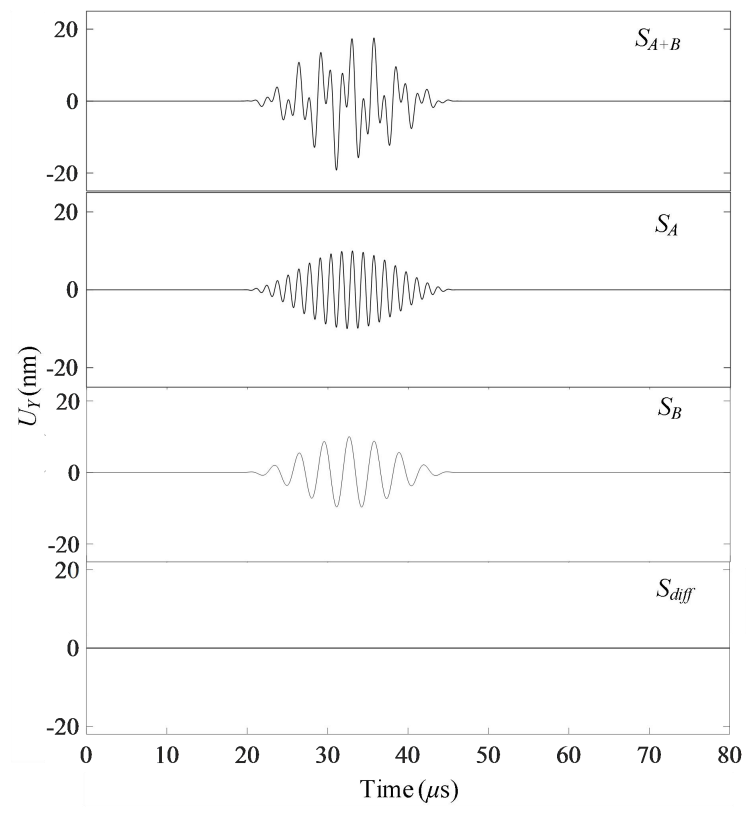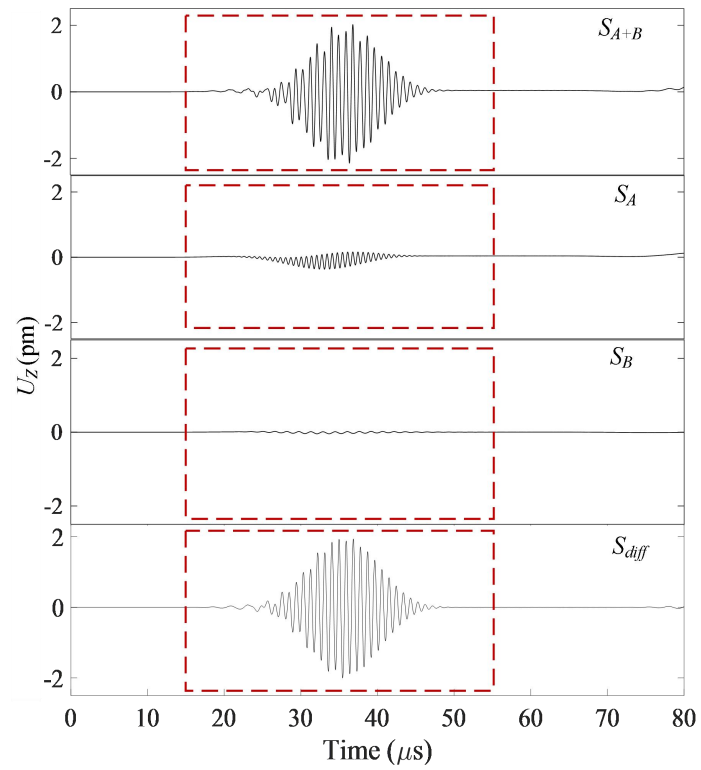
Fig. 3. Received signals at a point 60 mm away from the excitation: (a) in-plane displacements; (b) out-of-plane displacements; (c) frequency spectra of the windowed wave packages for S_A and S_B in (b); (d) frequency spectra of the windowed wave packages for S_{A+B} and S_{diff} in (b).

3.3 Cumulative effect of the secondary S0 Lamb wave

The cumulative effect of the generated nonlinear Lamb wave is investigated. Using the subtraction method, the nonlinear Lamb wave U_Z signals are extracted at different wave propagation distances from 20 mm to 120 mm in increments of 20 mm as shown in Fig. 4(a). A cumulative trend is clearly observed from the time-domain signals. To further quantify the cumulative effect, the peak amplitudes of the time-domain signals in Fig. 4(a) are plotted in Fig. 4(b). The results show a linear accumulation initially, which corresponds to when the three wave packets are fully interacting. After the waves propagate more than 80 mm the Lamb wave packets start to separate from the SH0 wave packets and the interaction decreases, which results in the Lamb wave amplitudes no longer increasing linearly. A simplified analytical model for the interaction of finite-sized wave packets having different group velocities was proposed by Hasanian and Lissenden [24]. The model shows that once the wave packets start to separate, the period increases and the amplitude increases less, which is apparent in Fig. 4(a).
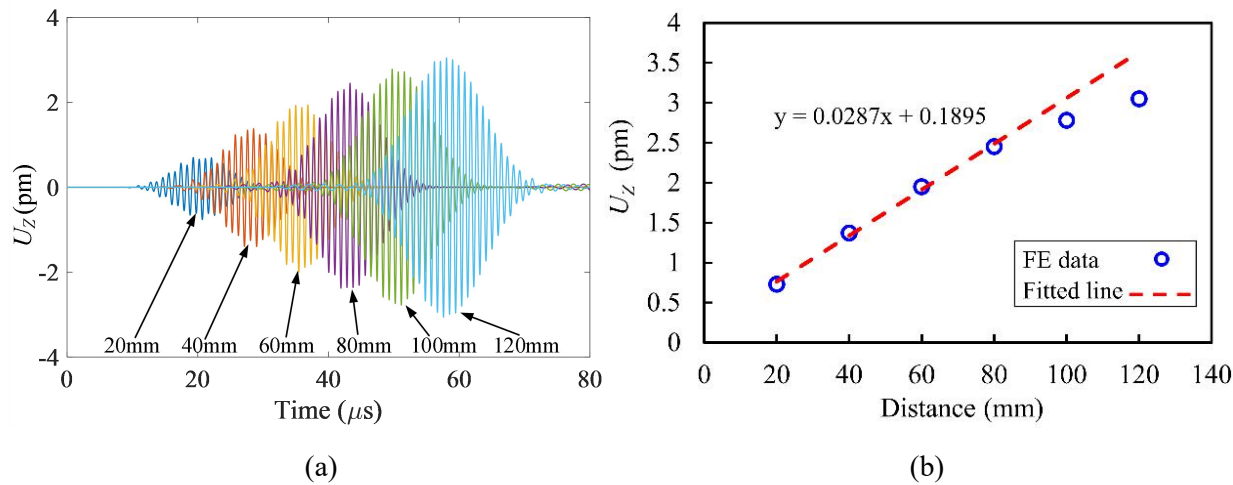

(a)   (b)

Fig. 4. Characterization of the cumulative effect of the nonlinear Lamb wave at the sum frequency: (a) the time-domain signals; (b) the extracted time-domain amplitudes.

3.4 Validation of the influence of the frequency combinations

The SH0 wave frequencies f_a and f_b that satisfy Eq. (15) are now assessed and the normalized value of β' computed from the finite element results using Eq. (19). The four sets of frequencies assessed are tabulated in Table 2 along with the values of mixing power M_{ir} [24]. In these cases, the amplitude and

time duration of all the primary waves are set to be the same at different frequencies. Using Eq. (19), the time-domain secondary Lamb wave signals are extracted for each of the four cases, as shown in Figs. 5(a) and (b). Similar wave packets are received for the four cases, which demonstrates that strong secondary Lamb waves at the sum-frequency are generated from different frequency combinations. Then, the amplitudes of the S0 wave components are obtained and the β' for the four cases are calculated according to Eq. (17). After normalizing with respect to Set 1, the β' values are plotted in Fig. 5(c). A clear increasing trend is observed when the frequencies of the primary SH0 waves are converging, which agrees with the theoretical analyses. Moreover, in the four cases, the wave numbers of the primary SH0 waves at different frequencies are calculated. The normalized β' with respect to the first case are then obtained and plotted against $k_a k_b$, in comparison with the theoretic prediction according to Eq. (18), as shown in Fig. 5(d). It is worth noting that $k_a k_b$ reaches the maximum when k_a equals to k_b according to Eq. (15). The FE data agree well with the theoretical prediction, which further validates the theoretical analyses.

Table 2. Frequency combinations of primary SH0 wave investigated in this work

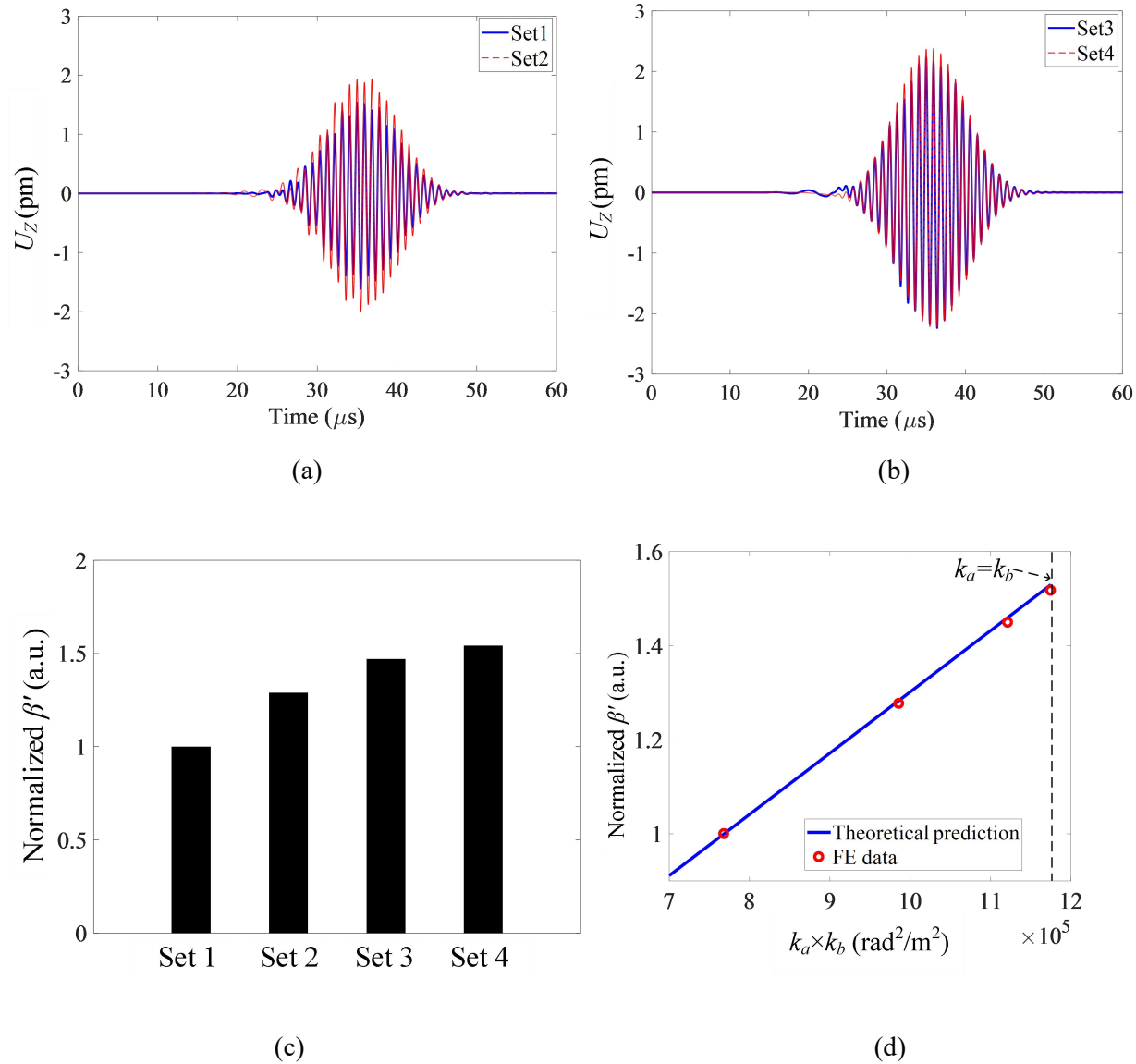| Set	f_a (MHz)	f_b (MHz)	$k_a k_b$ (rad^{2}m^{-2})	M_{ir} (m^{-2})
1	0.85	0.22	0.764×10^6	0.2891×10^6
2	0.75	0.32	0.982×10^6	0.3715×10^6
3	0.65	0.42	1.118×10^6	0.4230×10^6
4	0.55	0.52	1.172×10^6	0.4434×10^6
-	0.5344	0.5344	1.173×10^6	0.4439×10^6

Fig. 5. Influence of the frequency combinations of the primary SH0 waves on the nonlinear Lamb wave generation: (a) and (b) time-domain signals in the four cases; (c) normalized β' associated with the four cases; (d) comparison between theoretical and FE results.

In summary, the simulation results demonstrate that strong secondary S0 mode Lamb waves can be generated by mixing two codirectional SH0 waves. Additionally, the generated nonlinear S0 mode Lamb wave is proven to be cumulative with respect to the propagating distance. Finally, the largest amplitude

secondary S0 Lamb wave generated by mixing two codirectional SH0 waves occurs when the primary wave frequencies are very close together.

4. EXPERIMENTS

Experiments are carried out to assess the cumulative effect of the secondary S0 mode Lamb wave and then to apply the proposed method to indicate material degradation due to cyclic tensile loading. To accomplish the experimental goals a gel filter is designed to mitigate the influence of undesired nonlinearities in the test setup.

4.1 Experimental setup

The experimental setup is illustrated in Fig. 6(a). Two magnetostrictive transducers (MSTs) were used to generate SH0 wave packets having center frequencies of f_a = 0.75 MHz and f_b = 0.32 MHz in a 3.125 mm-thick 2024-T3 aluminum plate using the two independent channels of a Ritec (Warwick, Rhode Island, USA) SNAP 5000 system. The meander spacings of the electrical coils for MSTs A and B are 3.6 mm and 10 mm, respectively. A time delay of 15 μs was applied to the signal sent to MST A so that the SH0 wave packets travel as one. To minimize the measurement variability, the non-contact Lorentz force Electromagnetic Acoustic Transducer (EMAT) and air-coupled (AC) sensor (Ultran, State College, Pennsylvania, USA) were used, avoiding any inconsistent coupling between the transducer and the plate. Specifically, the EMAT designed for 250 kHz was used to measure the in-plane (U_Y) displacements associated with the SH waves, while the 1 MHz AC sensor received the out-of-plane (U_Z) displacements corresponding to the S0 Lamb wave at 1.07 MHz, which has significant out of plane displacement [17, 32]. The EMAT is used with zero liftoff and manually positioned for these tests. The AC sensor is mounted on a fixed stage. Instead of moving the transducer, we slide the plate relative to the AC sensor to measure the responses at different positions, which avoids any unexpected changes in the sensor configurations. In this case, the measurement variability can be minimized. The sampling rate of the system was set to 250 MHz, and 512 signals were averaged together. Damping materials were bonded to the edges of the plate to reduce the boundary reflections.

Although the wave mixing method is immune to instrument nonlinearities, there are other sources of nonlinearity in this specific configuration, especially at the actuating part [33, 34]. As shown in Fig. 6(b), the SH waves generated by the two MSTs must mix in the iron-cobalt foil of the MST as well as the epoxy adhesive (J-B Weld, Atlanta, Georgia, USA) bonding layer. Material nonlinearity from the foil and the epoxy could mask the material nonlinearity from the aluminum, which is the only nonlinearity we want to measure. This was not an issue in previous experiments using counter-propagating waves [17] because the waves did not mix in the MSTs. Therefore, it is crucial to confirm that the material nonlinearity of the plate plays a dominant role in the signal nonlinearities before any meaningful conclusions can be drawn. To tackle this problem, a simple gel filter is employed to mitigate the influence of any undesired nonlinear sources. The large U_Z displacement at the plate surface of the S0 Lamb mode at 1.07 MHz leaks into the liquid gel, effectively damping it out. But the gel has no effect on the SH0 mode. Thus, an ultrasound gel filter is placed on the top surface of the plate near the MST as shown in Fig. 6. The gel ensures that the S0 wave measured by the AC sensor is associated with nonlinearity of the aluminum sample, as will be demonstrated.
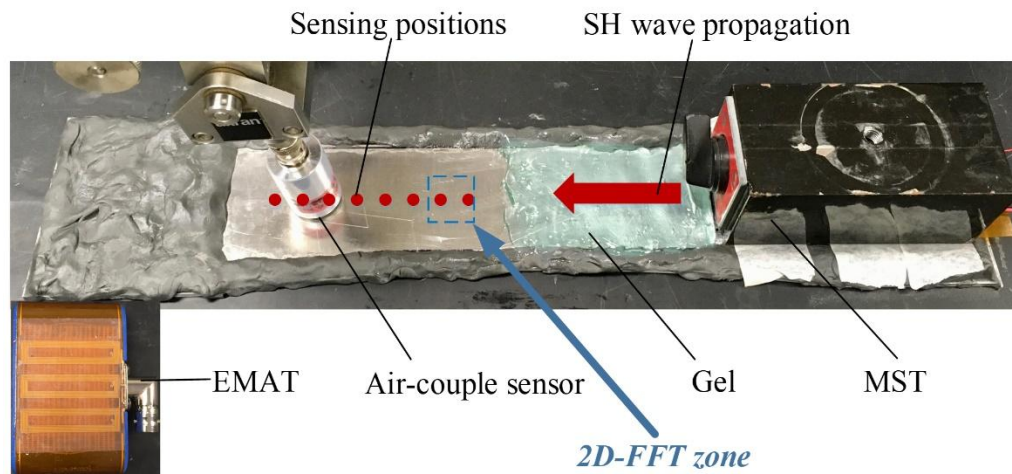
(a)
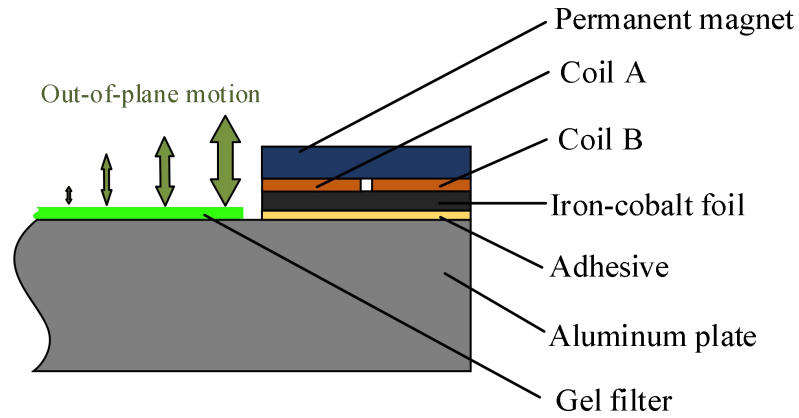
(b)

Fig. 6. Experimental setup for aluminum plate testing: (a) Photo showing AC sensor, dual MSTs, gel, putty, and measurement points; (b) cross-sectional sketch of wave actuation end of test setup.

4.2 Linear and nonlinear responses

First, the linear responses of the two individual SH waves A and B at different sensing points are captured with the EMAT as shown in Fig. 7, exemplified by the signals acquired with the edge of the EMAT housing 20, 50 and 80 mm from the end of the gel. The amplitudes of waves A and B can be considered independent of propagation distance between 20-80 mm, since the amplitude variations for waves A and B are just 5% and 2% respectively. Thus, the values of A_a and A_b in Eq. (16) are assumed to be constant over the range of measurements.
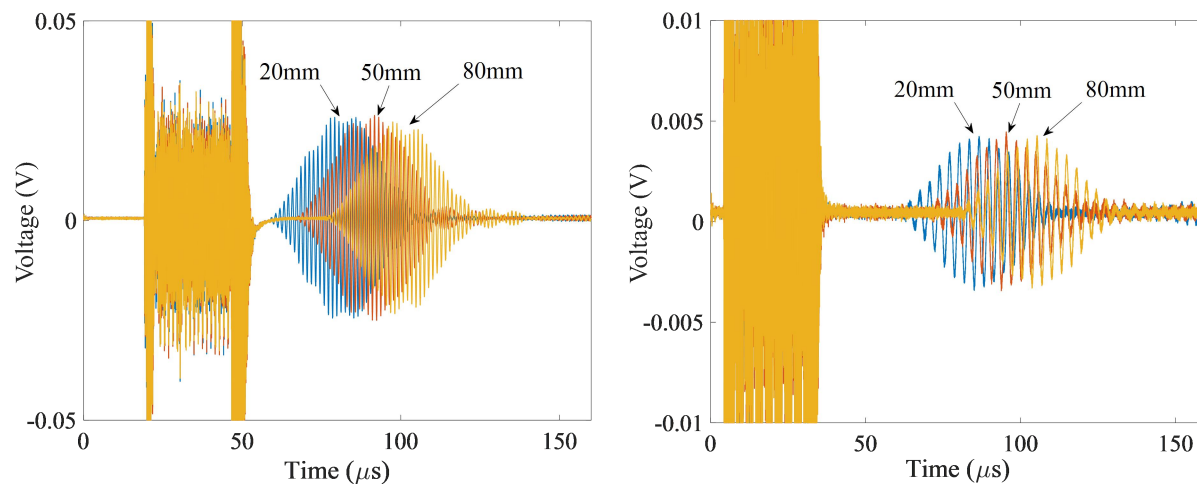
Fig. 7. The linear SH wave signals at different sensing positions captured from the EMATs: (a)

high-frequency wave *A*; (b) low-frequency wave *B*.

设置格式[Shan Shengbo]: 字体颜色: 红色

After measuring the primary wave amplitudes, the AC transducer is used to receive the nonlinear Lamb waves. Using the subtraction method (Eq. 19), the nonlinear Lamb wave signal is obtained, exemplified by the signal shown in Fig. 8(a), which was received 90 mm from the end of the gel. The FFT of the windowed signal in Fig. 8(a) gives the frequency spectrum plotted in Fig. 8(b), which indicates that the signal propagates with a center frequency of 1.07 MHz – the sum frequency of the primary waves, $f_a + f_b$.

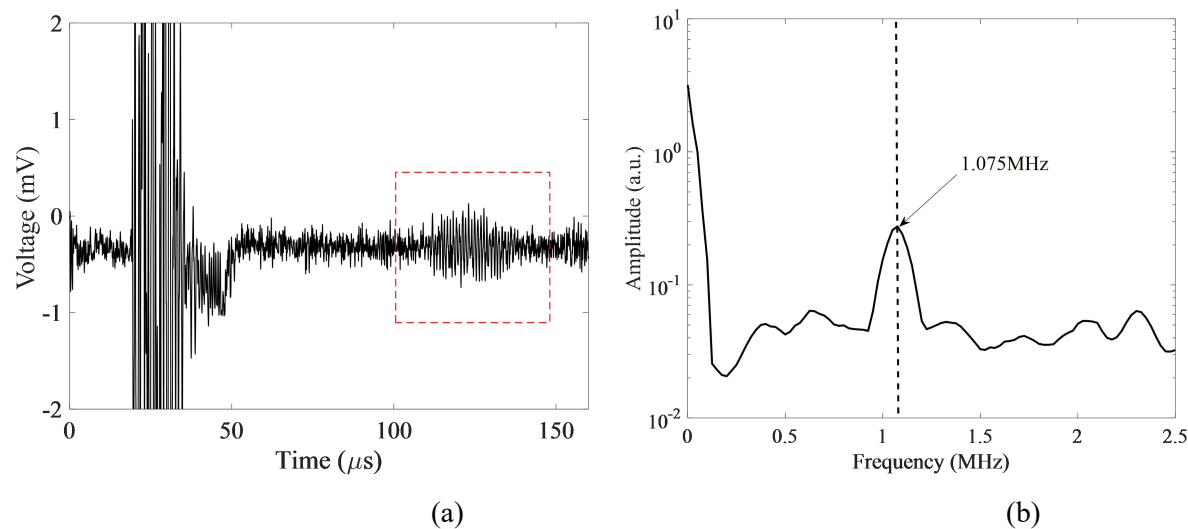(a)   (b)

Fig. 8. Difference signal computed by Eq. (19) from signals received by the AC sensor 90 mm away from

the end of the gel: (a) time-domain signal; (b) frequency spectrum of the windowed wave packet in (a).

4.3 Effect of the gel filter

Having identified the frequency of the received signal by FFT, the next check is to identify the propagating modes and the effect of the gel filter. A 2D-FFT analysis is carried out in a zone near the end of the gel, as illustrated in Fig. 6(a). In this zone, 16 sensing points at 1 mm intervals are used. After obtaining the 16 nonlinear Lamb wave responses using Eq. (19), the 2D-FFT analysis is performed to

study the wave components in the phase velocity-frequency domain [35-37]. Data are first acquired in the absence of the gel filter, and the 2D-FFT results are shown in Fig. 9(a). After simply placing the gel, the data acquisition is repeated and the corresponding results are plotted in Fig. 9(b). Results again show that the received nonlinear signals are at the sum frequency-thickness product, $(f_a + f_b)2h = 3.34$ MHz-mm. It is worth noting that due to the 1 mm spatial resolution, the calculated phase velocities have limited accuracy. However, some important information is provided. In comparing Figs. 9(a) and 9(b), it is clear that the gel filter damps a significant amount of the Lamb wave energy. Moreover, in the absence of gel, Lamb wave modes in addition to the S0 mode could be generated. After placing the gel, very little energy could propagate other than the S0 mode, which provides great benefit for analyses of material degradation within the waveguide.
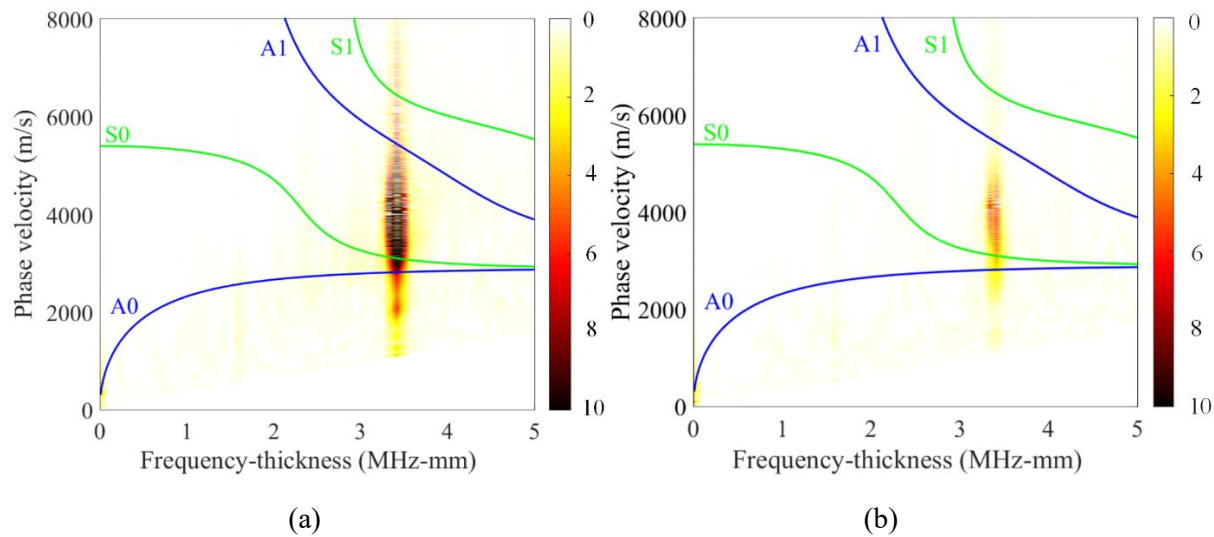

Fig. 9. 2D-FFT results superimposed on Lamb wave dispersion curves: (a) no gel; (b) with gel.

4.4 Cumulative effect of the sum harmonic Lamb wave

Experiments are conducted to assess whether the nonlinear Lamb wave is cumulative for this internally resonant wave triplet, as expected for the SH0 primary waves and S0 secondary waves employed. First, tests were conducted with the gel filter in place. According to the finite element result in Fig. 4(b), the linearly cumulative effect stops after the propagation distance of about 90 mm due to the group velocity

mismatch. Therefore, eight sensing points were selected from 20-90 mm away from the gel in 10 mm intervals, as shown by the red dots in Fig. 6(a). After extracting the difference signals with the subtraction method at each point, FFT analysis was used to determine the amplitude A_{ab} at the sum frequency. The results in Fig. 10(a) show a clear cumulative effect. Next, the gel filter was simply removed without changing anything else. Following the same process, the amplitudes A_{ab} at different locations are plotted in Fig. 10(b). In this case, the amplitudes are larger, but no cumulative effect is observed, suggesting that the material nonlinearity is overwhelmed by other nonlinear sources. This demonstrates the importance of the gel filter in the system design. Moreover, the nonlinear wave amplitudes with respect to the propagation distance in Fig. 10(a) can be fitted with a line whose slope is indicative of material nonlinearity within the waveguide.
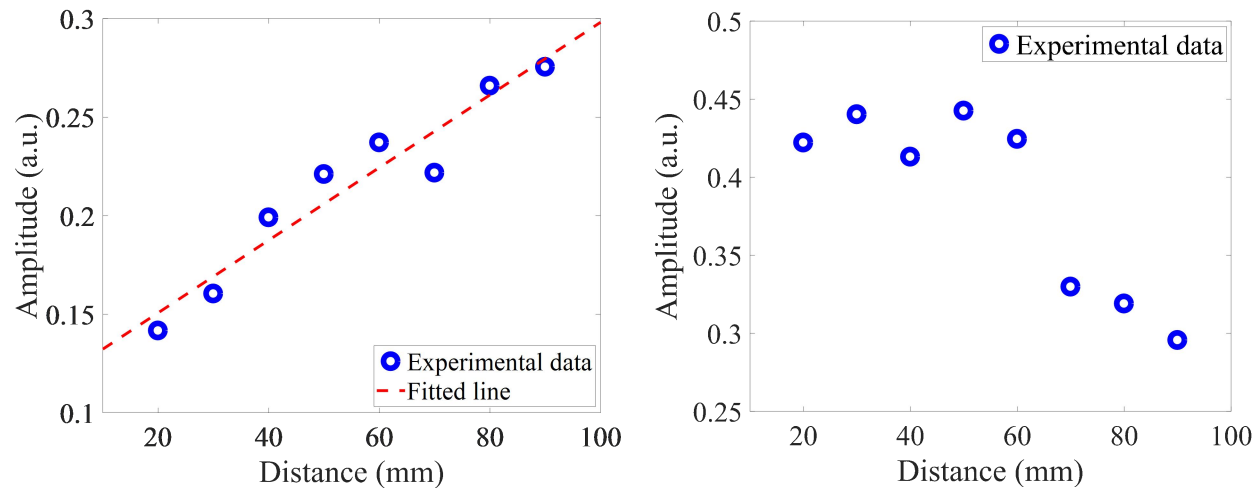

Fig. 10. Amplitude A_{ab} obtained from the difference signal computed from the AC sensor as a function of propagation distance: (a) with the gel filter; (b) without the gel filter.

4.5 Characterization of fatigued structures

According to the theoretical analysis resulting in Eqs. (18) and (A13), the slope β'/X associated with the cumulative effect only depends on the parameter C (given the primary wave numbers k_a and k_b), which in turn is related to the Landau TOECs $\overline{A}$ and $\overline{B}$. Therefore, any changes in the TOECs resulting from material degradation can be characterized by the slope β'/X. In other words, material degradation can be detected using

this nonlinear ultrasonic technique by tracking changes in this slope. The proposed method is applied to fatigue in plate samples below.

A set of aluminum plate samples were subjected to increasing numbers of tensile loading cycles (maximum stress = yield strength, stress ratio = 0.1), creating fatigue damage but no visible cracks. First, cyclic loading was applied to a 3.125 mm thick 2024-T3 aluminum plate sample with a servohydraulic test frame until it fractured. Then cycling to 25%, 50% and 75% of the fatigue life was applied to three identical plate samples. The ultrasound measurements described above were taken on a pristine sample and the three fatigued samples; the fractured sample was not tested ultrasonically. The gel filter was used in all tests and measurements were made at the same eight sensing points described above (i.e., 20-90 mm from the end of the gel). Using the same procedure, the amplitude A_{ab} of the sum frequency is plotted as a function of the propagation distance in Fig. 11(a) and linear regression is used to determine the slope for each of the four samples. The coefficients of determination R^2 are also obtained and shown in Fig. 11(a), indicating a good linearity for all the four samples. Then, the slopes are normalized with respect to the values obtained from the pristine sample and plotted as a function of percentage of fatigue life. Four independent sets of measurements were made, then the mean and standard deviation were plotted in Fig. 11(b).

The results show a dramatic increase in the slopes; around 20% increase after the plate is fatigued to just 25% of its life. The slope increases 45% for the sample fatigued to 75% of its life. No cracks were observed by visual inspection of the samples. The changes in slopes demonstrate the effectiveness of the proposed nonlinear method for early damage detection and evaluation. In addition, as the amplitudes of the measurement errors are much smaller than the changes in the slopes, it is demonstrated the changes from the material degradations are more important than that induced by measurement variability.
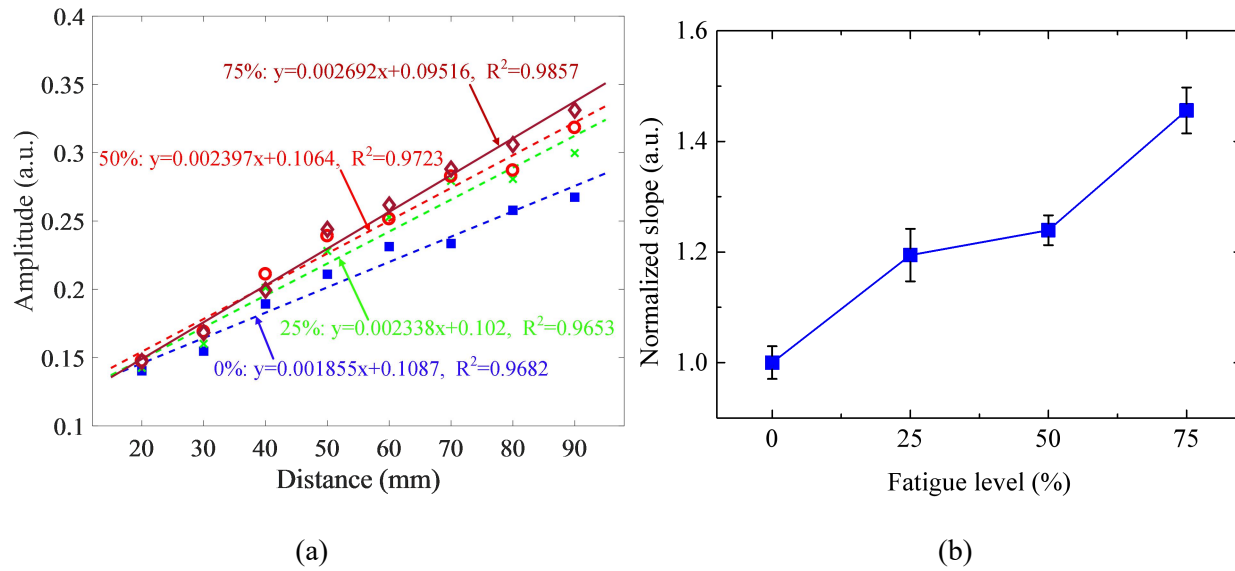
Fig. 11. (a) Amplitude A_{ab} obtained from the difference signal computed from the AC sensor as a function of propagation distance for aluminum plates cycled to 0, 25, 50, and 75% of the fatigue life; (b) normalized slope of the amplitude versus distance curve for the four samples.

The experiments demonstrate that codirectional mixing of two primary waves can effectively generate secondary S0 Lamb waves at the sum frequency. A gel filter was used to eliminate unwanted nonlinearities, most likely caused by the transducer materials. The secondary Lamb waves increase in amplitude while the waves are interacting and the slope of the Lamb wave amplitude as a function of propagation distance appears to correlate with material degradation due to fatigue. Most importantly, the method has high sensitivity to early material degradation.

Conclusions

A nonlinear ultrasonic method was proposed based on a group of newly discovered wave triplets where two codirectional propagating SH0 waves mix and generate a cumulative secondary S0 Lamb wave at the sum frequency. To validate the proposed method, finite element simulations were conducted and a subtraction method used to extract nonlinear features. The secondary S0 Lamb wave amplitude increased with propagation distance. Experiments were then carried out and the received secondary S0 Lamb waves

were sensitive to material degradation associated with fatigue in an aluminum plate.

The newly discovered wave triplets include all frequency combinations of the primary SH0 waves that sum to the frequency at which the SH0 and S0 dispersion curves intersect and the secondary S0 Lamb wave. Both theoretical and finite element modeling indicated that the closer together the primary frequencies, the more efficient the generation of the secondary S0 Lamb wave. In addition, finite element simulations and experimental results confirm the cumulative nature of the secondary S0 Lamb waves. Modeling of the wave interactions revealed that the normalized slope of the cumulative secondary wave as a function of propagation distance is influenced by two third-order elastic constants. Thus, a relatively direct correlation between measured ultrasonic nonlinearity and material constants exists and can be utilized in practical ways for nondestructive characterization of plate-like structures.

Based on the above findings, some appealing characteristics of the proposed method for further NDE applications are highlighted as follows. First, it offers great flexibility in terms of the selection of the excitation frequencies. Moreover, guided by the evaluation of the frequency combinations, it becomes possible to design optimal NDE systems with high nonlinear wave generation efficiency. Second, due to the different polarization characteristics between the primary SH0 waves and the secondary S0 wave, the nonlinear waves can be separated from the primary waves to simplify measurements. Third, the designed gel filter provides effective mitigation of unwanted nonlinearity from actuation, which might otherwise overwhelm the material nonlinearity of interest. Fourth, in addition to the strong second harmonic energy resulting from large wave mixing region, the proposed method also provides high sensitivity to global material degradation. Therefore, based on its strong potential it deserves further development for the engineering applications.

Acknowledgments

152070/16E).

References

[1]   K.-Y. Jhang,Nonlinear ultrasonic techniques for nondestructive assessment of micro damage in material: a review, Int. J. Precis. Eng. Manuf. 10 (1) (2009) 123-135.

[2]   A.J. Croxford, Wilcox P.D., Drinkwater B.W. and Nagy P.B.,The use of non-collinear mixing for nonlinear ultrasonic detection of plasticity and fatigue, J. Acous. Soc. Am. 126 (5) (2009) El117-El122.

[3]   V.K. Chillara and Lissenden C.J.,Review of nonlinear ultrasonic guided wave nondestructive evaluation: theory, numerics, and experiments, Opt. Eng. 55 (1) (2015) 011002.

[4]   K. Matlack, Kim J.-Y., Jacobs L. and Qu J.,Review of second harmonic generation measurement techniques for material state determination in metals, J. Nondestr. Eval. 34 (1) (2015) 273.

[5]   G. Tang, Liu M., Jacobs L.J. and Qu J.,Detecting localized plastic strain by a scanning collinear wave mixing method, J. Nondestr. Eval. 33 (2) (2014) 196-204.

[6]   J. Potter, Croxford A. and Wilcox P.,Nonlinear ultrasonic phased array imaging, Phys. Rev. Lett. 113 (14) (2014) 144301.

[7]   H.J. Lim, Song B., Park B. and Sohn H.,Noncontact fatigue crack visualization using nonlinear ultrasonic modulation, NDT&E Int. 73 (2015) 8-14.

[8]   A. Hikata, Chick B.B. and Elbaum C.,Dislocation contribution to the second harmonic generation of ultrasonic waves, J. Appl. Phys. 36 (1) (1965) 229-236.

[9]   K. Scott, Kim J.-Y. and Jacobs L.J.,Signal processing methods for second harmonic generation in thin specimens, NDT&E Int. 95 (2018) 57-64.

[10]   Y. Liu, Chillara V.K. and Lissenden C.J.,On selection of primary modes for generation of strong internally resonant second harmonics in plate, J. Sound Vib. 332 (19) 2013 4517-4528.

[11]   G.L. Jones and Kobett D.R.,Interaction of elastic waves in an isotropic solid, J. Acous. Soc. Am. 35 (1) 1963 5-10.

[12]   V. Korneev and Demčenko A.,Possible second-order nonlinear interactions of plane waves in an elastic solid, J. Acous. Soc. Am. 135 (2) 2014 591-598.

[13]   M.B. Morlock, Kim J.-Y., Jacobs L.J. and Qu J.,Mixing of two co-directional Rayleigh surface waves in a nonlinear elastic material, J. Acous. Soc. Am. 137 (1) 2015 281-292.

[14]   Z. Chen, Tang G., Zhao Y., Jacobs L.J. and Qu J.,Mixing of collinear plane wave pulses in elastic solids with quadratic nonlinearity, J. Acous. Soc. Am. 136 (5) 2014 2389-2404.

[15]   A. Demčenko, Akkerman R., Nagy P. and Loendersloot R.,Non-collinear wave mixing for non-linear ultrasonic detection of physical ageing in PVC, NDT&E Int. 49 2012 34-39.

[16]   M. Liu, Tang G., Jacobs L.J. and Qu J.,Measuring acoustic nonlinearity parameter using collinear wave mixing, J. Appl. Phys. 112 (2) 2012 024908.

[17]   M. Hasanian and Lissenden C.J.,Second order harmonic guided wave mutual interactions in plate: Vector analysis, numerical simulation, and experimental results, J. Appl. Phys. 122 (8) 2017 084901.

[18]   Z. Zhang, Nagy P.B. and Hassan W.,Analytical and numerical modeling of non-collinear shear

wave mixing at an imperfect interface, Ultrasonics 65 2016 165-176.

[19] N. Kalayanasundaram,Nonlinear mode coupling of surface acoustic waves on an isotropic solid, Int. J. Eng. Sci. 19 (3) 1981 435-441.

[20] W. De Lima and Hamilton M.,Finite-amplitude waves in isotropic elastic plates, J. Sound Vib. 265 (4) 2003 819-839.

[21] V. Krishna Chillara and Lissenden C.J.,Interaction of guided wave modes in isotropic weakly nonlinear elastic plates: Higher harmonic generation, J. Appl. Phys. 111 (12) 2012 124909.

[22] Y. Liu, Lissenden C.J. and Rose J.L.,Higher order interaction of elastic waves in weakly nonlinear hollow circular cylinders. I. Analytical foundation, J. Appl. Phys. 115 (21) 2014 214901.

[23] Y. Liu, Khajeh E., Lissenden C.J. and Rose J.L.,Higher order interaction of elastic waves in weakly nonlinear hollow circular cylinders. II. Physical interpretation and numerical results, J. Appl. Phys. 115 (21) 2014 214902.

[24] M. Hasanian and Lissenden C.J.,Second order ultrasonic guided wave mutual interactions in plate: Arbitrary angles, internal resonance, and finite interaction region, J. Appl. Phys. 124 (2018), in press.

[25] B.A. Auld, Acoustic fields and waves in solids, Robert E. Krieger, 1990.

[26] H.J. Lim, Sohn H. and Kim Y.,Data-driven fatigue crack quantification and prognosis using nonlinear ultrasonic modulation, Mech. Syst. Signal Process. 109 (2018) 185-195.

[27] M. Sun, Xiang Y., Deng M., Xu J. and Xuan F.-Z.,Scanning non-collinear wave mixing for nonlinear ultrasonic detection and localization of plasticity, NDT&E Int. 93 2018 1-6.

[28] J. Jingpin, Xiangji M., Cunfu H. and Bin W.,Nonlinear Lamb wave-mixing technique for micro-crack detection in plates, NDT&E Int. 85 2017 63-71.

[29] P.M. Thanseer, Metya A.K. and Sagar S.P.,Development of a Non-collinear Nonlinear Ultrasonic-Based Technique for the Assessment of Crack Tip Deformation, J. Mater. Eng. Perform. 26 (6) 2017 2632-2639.

[30] F. Li, Zhao Y., Cao P. and Hu N.,Mixing of ultrasonic Lamb waves in thin plates with quadratic nonlinearity, Ultrasonics 87 2018 33-43.

[31] Wu W, Owino J, Al-Ostaz A, et al. Applying periodic boundary conditions in finite element analysis. SIMULIA Community Conference, Providence, 2014.

[32] J.L. Rose, Ultrasonic guided waves in solid media, Cambridge university press, 2014.

[33] A. Mostavi, Kabir M. and Ozevin D.,The integration of superlattices and immersion nonlinear ultrasonics to enhance damage detection threshold, Appl. Phys. Lett. 111 (20) 2017 201905.

[34] S. Shan, Cheng L. and Li P.,Adhesive nonlinearity in Lamb-wave-based structural health monitoring systems, Smart Mater. Struct. 26 (2) 2016 025019.

[35] B. Ren and Lissenden C.J.,PVDF multielement lamb wave sensor for structural health monitoring, IEEE T. Ultrason. Ferr. 63 (1) 2016 178-185.

[36] D. Alleyne and Cawley P.,A two-dimensional Fourier transform method for the measurement of propagating multimode signals, J. Acous. Soc. Am. 89 (3) 1991 1159-1168.

[37] J.-G. Minonzio, Talmant M. and Laugier P.,Guided wave phase velocity measurement using multi-emitter and multi-receiver arrays in the axial transmission configuration, J. Acous. Soc. Am.

Appendix

For the case of wave mixing, when substituting $(\mathbf{u}_a + \mathbf{u}_b)$ into Eq. (5), the nonlinear stress term corresponding to mutual wave interaction becomes

$$\mathbf{S}^{NL}(\boldsymbol{a}, \boldsymbol{b}) = \frac{\lambda}{2} tr[\mathbf{H}_b + \mathbf{H}_b^T]\mathbf{H}_a + \mu\mathbf{H}_a(\mathbf{H}_b + \mathbf{H}_b^T) + \frac{\lambda}{2} tr[\mathbf{H}_a + \mathbf{H}_a^T]\mathbf{H}_b + \mu\mathbf{H}_b(\mathbf{H}_a + \mathbf{H}_a^T) + \frac{\lambda}{2} tr[\mathbf{H}_b^T\mathbf{H}_a +$$

$$\mathbf{H}_a^T\mathbf{H}_b]\mathbf{I} + 2\bar{C}tr[\mathbf{H}_a]tr[\mathbf{H}_b]\mathbf{I} + \mu(\mathbf{H}_b^T\mathbf{H}_a + \mathbf{H}_a^T\mathbf{H}_b) + \bar{B}tr[\mathbf{H}_a](\mathbf{H}_b + \mathbf{H}_b^T) + \bar{B}tr[\mathbf{H}_b](\mathbf{H}_a + \mathbf{H}_a^T) +$$

$$\frac{\bar{B}}{2} tr[\mathbf{H}_a\mathbf{H}_b + \mathbf{H}_b\mathbf{H}_a + \mathbf{H}_b^T\mathbf{H}_a + \mathbf{H}_a^T\mathbf{H}_b]\mathbf{I} + \frac{\bar{A}}{4}(\mathbf{H}_a\mathbf{H}_b + \mathbf{H}_b\mathbf{H}_a + \mathbf{H}_a^T\mathbf{H}_b^T + \mathbf{H}_b^T\mathbf{H}_a^T + \mathbf{H}_b^T\mathbf{H}_a + \mathbf{H}_a^T\mathbf{H}_b +$$

$$\mathbf{H}_a\mathbf{H}_b^T + \mathbf{H}_b\mathbf{H}_a^T). \tag{A1}$$

For the special case of codirectional SH0 wave mixing the displacement wave fields are given by

$$\mathbf{u}_a = \begin{bmatrix} 0 \\ 1 \\ 0 \end{bmatrix} A_a e^{i(k_a X - \omega_a t)} \tag{A2}$$

$$\mathbf{u}_b = \begin{bmatrix} 0 \\ 1 \\ 0 \end{bmatrix} A_b e^{i(k_b X - \omega_b t)} \tag{A3}$$

and the displacement gradients are

$$\mathbf{H}_a = \begin{bmatrix} 0 & 0 & 0 \\ i & 0 & 0 \\ 0 & 0 & 0 \end{bmatrix} A_a k_a e^{i(k_a X - \omega_a t)} \tag{A4}$$

$$\mathbf{H}_b = \begin{bmatrix} 0 & 0 & 0 \\ i & 0 & 0 \\ 0 & 0 & 0 \end{bmatrix} A_b k_b e^{i(k_b X - \omega_b t)}. \tag{A5}$$

Now substitute Eqs. (A4) and (A5) into Eq. (A1) to obtain the nonlinear stress term and then take its divergence,

$$\mathbf{S}^{NL}(\boldsymbol{a}, \boldsymbol{b}) = -A_a A_b k_a k_b e^{i((k_a+k_b)X - (\omega_a+\omega_b)t)} \begin{bmatrix} \lambda + 2\mu + \bar{B} + \dfrac{\bar{A}}{2} & \dfrac{\bar{A}}{2} & 0 \\ \dfrac{\bar{A}}{2} & \lambda + 2\mu + \bar{B} + \dfrac{\bar{A}}{2} & 0 \\ 0 & 0 & \lambda + \bar{B} \end{bmatrix}$$

(A6)

$$Div[\mathbf{S}^{NL}(\mathbf{a},\mathbf{b})] =- iA_aA_b(k_a+k_b)k_ak_be^{i((k_a+k_b)X-(\omega_a+\omega_b)t)}\left[\lambda+2\mu+\overline{B}+\frac{\overline{A}}{2} \quad \frac{\overline{A}}{2} \quad 0\right]. \quad (A7)$$

In addition, the secondary S0 mode Lamb wave will have the velocity field

$$\mathbf{V}_m = \begin{bmatrix} V_{mX}(Z) \\ 0 \\ V_{mZ}(Z) \end{bmatrix} A_m e^{i(k_mX-\omega_mt)} \qquad (A8)$$

where $V_{mx}(Z)$ and $V_{mz}(Z)$ denote the displacement profile through the thickness. The nonlinear driving

forces can now be written explicitly by substituting Eqs. (A6) – (A8) into Eqs. (10) and (11)

$$f_m^{surf} = (\lambda+\overline{B})A_aA_bk_ak_bV_{mZ}^*(h) \qquad (A9)$$

$$f_m^{vol} =- i\left(\lambda+2\mu+\overline{B}+\frac{\overline{A}}{2}\right)A_aA_b(k_a+k_b)k_ak_b\int_0^h V_{mX}^*(Z)\,dZ. \qquad (A10)$$

Finally, the amplitude of the cumulative secondary S0 Lamb wave is obtained by substituting Eqs. (A9)

and (A10) into Eq. (9),

$$A_m(X) = A_aA_bk_ak_bX\left(\frac{(\lambda+\overline{B})V_{mZ}^*(h)-i\left(\lambda+2\mu+\overline{B}+\frac{\overline{A}}{2}\right)(k_a+k_b)\int_0^h V_{mX}^*(Z)\,dZ}{4P_{mm}}e^{i(k_a\pm k_b)X}\right) \qquad (A11)$$

Therefore, the amplitude of the S0 mode in Eq. (8) generated by the mutual interaction of two

codirectional SH0 waves can be written simply as

$$A_{ab} = C(A_aA_b)(k_ak_b)X \qquad (A12)$$

with

$$C = \left|\frac{(\lambda+\overline{B})V_{mZ}^*(h)-i\left(\lambda+2\mu+\overline{B}+\frac{\overline{A}}{2}\right)(k_a+k_b)\int_0^h V_{mX}^*(Z)\,dZ}{8P_{mm}}\right|. \qquad (A13)$$

All of the SH0 primary wave combinations considered in this work generate the S0 mode at the same

frequency-thickness product and the same (k_a+k_b) value. Thus, C can simply treated as a constant.